

Towards Reliable Evaluation of Adversarial Robustness for Spiking Neural Networks

Jihang Wang^{1,2}Dongcheng Zhao¹Ruolin Chen^{1,2}Qian Zhang^{1,2,3,4,5*}Yi Zeng^{1,2,3,4,5*}¹Brain-inspired Cognitive AI Lab, Institute of Automation, Chinese Academy of Sciences²School of Artificial Intelligence, University of Chinese Academy of Sciences³Beijing Institute of AI Safety and Governance⁴Beijing Key Laboratory of Safe AI and Superalignment⁵Center for Long-term AI

{wangjihang2021, chenruolin2024, q.zhang, yi.zeng}@ia.ac.cn

zhaodc@ion.ac.cn

Abstract

Spiking Neural Networks (SNNs) utilize spike-based activations to mimic the brain’s energy-efficient information processing. However, the binary and discontinuous nature of spike activations causes vanishing gradients, making adversarial robustness evaluation via gradient descent unreliable. While improved surrogate gradient methods have been proposed, their effectiveness under strong adversarial attacks remains unclear. We propose a more reliable framework for evaluating SNN adversarial robustness. We theoretically analyze the degree of gradient vanishing in surrogate gradients and introduce the Adaptive Sharpness Surrogate Gradient (ASSG), which adaptively evolves the shape of the surrogate function according to the input distribution during attack iterations, thereby enhancing gradient accuracy while mitigating gradient vanishing. In addition, we design an adversarial attack with adaptive step size under the L_∞ constraint—Stable Adaptive Projected Gradient Descent (SA-PGD), achieving faster and more stable convergence under imprecise gradients. Extensive experiments show that our approach substantially increases attack success rates across diverse adversarial training schemes, SNN architectures and neuron models, providing a more generalized and reliable evaluation of SNN adversarial robustness. The experimental results further reveal that the robustness of current SNNs has been significantly overestimated and highlighting the need for more dependable adversarial training methods.

1. Introduction

Spiking Neural Networks (SNNs) have emerged as brain-inspired models that emulate the sparse, event-driven processing of biological neural systems [4, 14, 32, 35, 36]. By transmitting information through discrete spikes instead of continuous activations, SNNs achieve high energy efficiency and rich temporal dynamics, making them attractive for neuromorphic and low-power applications [7, 23, 28, 30, 31]. However, the discontinuous and binary nature of spike activations hinders the application of gradient-based adversarial attacks, making reliable robustness evaluation difficult [1].

To overcome the non-differentiability of spike activations, surrogate gradient methods approximate the spike derivative with a smooth function [26, 32]. While this enables backpropagation, it introduces approximation errors that distort gradients, especially under adversarial perturbations where accurate input gradients are essential [1, 2]. As a result, gradient-based robustness evaluation in SNNs remains unreliable.

Several studies have refined surrogate gradients [3, 15, 22, 34], yet existing methods lack input-dependent designs and theoretical analysis of gradient vanishing. Moreover, most works overlook the development of constrained optimization algorithms for adversarial attacks, which are equally crucial for reliable robustness evaluation.

In this work, we propose a reliable framework for evaluating the adversarial robustness of SNNs from both the gradient approximation and attack optimization perspectives. Specifically, we first theoretically analyze the degree of gradient vanishing inherent in surrogate gradient functions

*Corresponding author.

of different shapes and introduce the Adaptive Sharpness Surrogate Gradient (ASSG). ASSG adaptively adjusts the sharpness of the surrogate gradient function according to the input distribution during attack iterations, enabling the surrogate gradient to closely approximate the true gradient while effectively mitigating gradient vanishing. Furthermore, we develop the Stable Adaptive Projected Gradient Descent (SA-PGD), an adversarial attack method that incorporates adaptive step-size adjustment under the L_∞ constraint, enabling faster and more stable convergence even when gradients are inaccurate. Our main contributions are summarized as follows:

- We theoretically derive the upper bound of the gradient-vanishing degree in surrogate gradient functions during adversarial attack process. Based on this analysis, we propose the Adaptive Sharpness Surrogate Gradient (ASSG). ASSG computes an input-dependent surrogate gradient that adaptively evolves during adversarial optimization, enabling the estimation of highly accurate gradients while effectively avoiding vanishing gradients.
- We design a new adversarial optimization algorithm with adaptive step-size control, which achieves more stable and efficient convergence even when gradients are imprecise.
- Extensive experiments across various SNN adversarial training schemes, neuron models, and architectures demonstrate that our approach substantially improves the effectiveness of adversarial attacks and generalizes well to different SNN configurations.
- Our findings reveal that the adversarial robustness of current SNNs has been significantly overestimated, highlighting the urgent need to rethink how to efficiently generate reliable adversarial samples for training more genuinely robust SNN models.

2. Related Works

2.1. Gradient Approximation Methods in SNNs

Recent studies have shown that SNNs are vulnerable to adversarial perturbations [8, 20]. Surrogate gradient methods approximate the spike activation with a continuous function to enable Spatial-Temporal Backpropagation (STBP) [32]. The Potential-Dependent Surrogate Gradient (PDSG) method further incorporates the variance of membrane potential distributions into the surrogate computation [22]. However, PDSG derives the surrogate function from batch-level statistics rather than individual samples, preventing adaptive modeling of sample-specific dynamics and lacking theoretical justification for its formulation.

Another line of research estimates input gradients by differentiating the SNN loss with respect to neurons’ average firing rates. Representative methods include Backward Pass Through Rate (BPTR) [8] and Rate Gradient Approxima-

tion (RGA) [3]. The Hybrid Adversarial attack based on Rate and Temporal information (HART) [15] jointly considers rate- and time-based dependencies, but its derivation is limited to a specific neuronal model and lacks theoretical validation for generalization to broader neuron types.

2.2. Adversarial Defense Methods for SNNs

Early studies adapted adversarial training for SNNs, such as adversarial input augmentation and min–max optimization [24]. Later approaches, including Regularized Adversarial Training (RAT), constrain the Lipschitz constant of each layer via weight regularization to stabilize learning [8], while Sparsity Regularization (SR) introduces a sparse gradient penalty into the loss to enhance robustness when combined with adversarial training [21].

More recent works have strengthened SNN adversarial defense from an architectural perspective [10, 33]. For instance, synaptic gating mechanisms dynamically regulate spike transmission to suppress adversarial noise propagation [10], and frequency-domain encoding schemes improve robustness by representing spiking information in more stable spectral domains [33].

3. Preliminaries

3.1. Adversarial Attack and Training

Adversarial attacks can be viewed as a constrained optimization problem in the input space of a neural network [5, 6, 11, 24, 25]. For a classification model $f_\theta : \mathbb{R}^d \rightarrow \mathbb{R}^C$, let $\mathbf{x} \in \mathbb{R}^d$ denote a benign input sample with the ground-truth label y . The objective of an untargeted adversarial attack is to find a perturbed input \mathbf{x}' that maximizes the classification loss \mathcal{L} while remaining within a small L_p -norm ball around the original input:

$$\mathbf{x}' = \arg \max_{\|\mathbf{x}' - \mathbf{x}\|_p \leq \varepsilon} \mathcal{L}(f_\theta(\mathbf{x}'), y) \quad (1)$$

here, ε defines the perturbation bound that controls the perceptual similarity between \mathbf{x} and \mathbf{x}' . In practice, gradient-based optimization methods such as Projected Gradient Descent (PGD) and Auto-PGD (APGD) are commonly used to approximate the solution of this problem under various norm constraints (e.g. L_∞ , L_2) [6, 24].

Adversarial Training (AT) is one of the most fundamental methods for improving a network’s adversarial robustness, and it has also been widely adopted in SNN-related studies [8–10, 18, 21, 27, 33]. The objective of AT can be formulated as a min–max optimization problem:

$$\min_{\theta} \mathbb{E}_{(\mathbf{x}, y) \sim \mathcal{D}} \left[\max_{\|\mathbf{x}' - \mathbf{x}\|_p \leq \varepsilon} \mathcal{L}(f_\theta(\mathbf{x}'), y) \right] \quad (2)$$

where \mathcal{D} denotes the data distribution. TRadeoff-inspired Adversarial DEfense via Surrogate-loss minimiza-

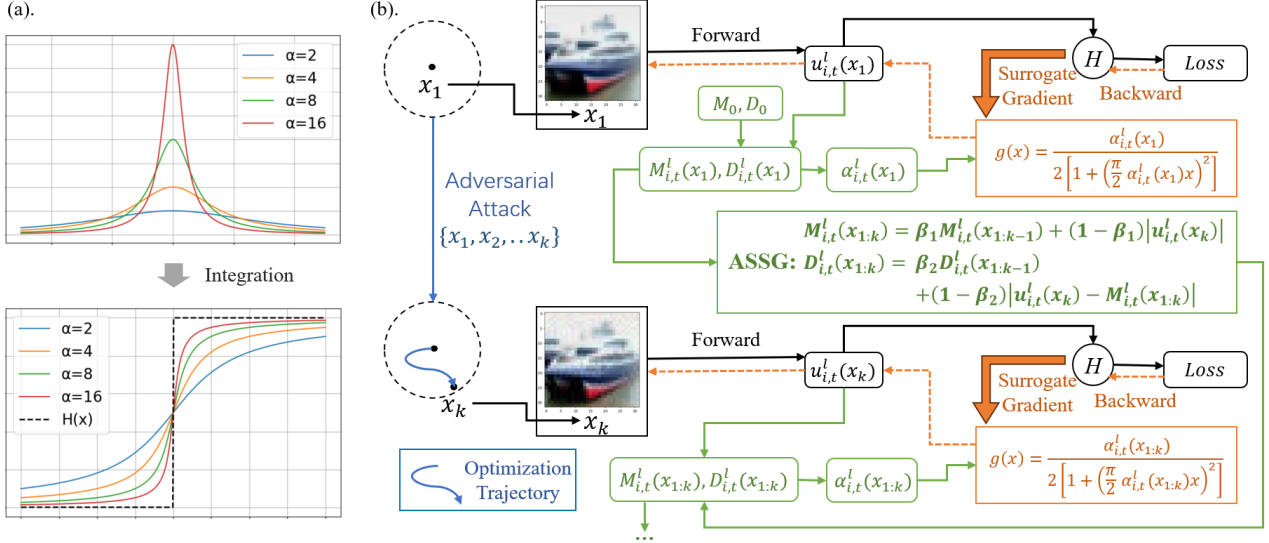


Figure 1. (a). Curves of the surrogate gradient function $g(x)$ and its integral under different sharpness parameters α . (b). Illustration of the adaptive mechanism of the surrogate gradient sharpness parameter in ASSG during adversarial attacks.

tion (TRADES) is one of the most influential variants of AT [29, 37], which is also employed as a training framework for developing robust SNNs in this work.

3.2. Spiking Neurons and Surrogate Gradients

Each neuron in SNN integrates incoming currents into its membrane potential and generates a spike once the potential exceeds a firing threshold:

$$\mathbf{V}^l(t+1) = F \left[R(\mathbf{V}^l(t), \mathbf{s}^l(t)), \mathbf{W}^l \mathbf{s}^{l-1}(t+1) \right] \quad (3)$$

$$\mathbf{s}^l(t+1) = H(\mathbf{V}^l(t+1) - V_{\text{th}}) \quad (4)$$

where $\mathbf{V}^l(t)$, $\mathbf{s}^l(t)$, and \mathbf{W}^l denote the membrane potential, spike output, and synaptic weight matrix in layer l at time step t , respectively. $H(x)$ is the Heaviside step function. $F(\cdot)$ and $R(\cdot)$ represent the membrane potential update and reset mechanisms, respectively. Different neuron models adopt different definitions for these two functions.

In this paper, we primarily employ the Leaky Integrate-and-Fire (LIF) neuron model:

$$\mathbf{V}^l(t+1) = \lambda R(\mathbf{V}^l(t), \mathbf{s}^l(t)) + (1 - \lambda) \mathbf{W}^l \mathbf{s}^{l-1}(t+1), \quad (5)$$

$$R(\mathbf{V}^l(t), \mathbf{s}^l(t)) = \begin{cases} 0, & \mathbf{s}^l(t) = 1, \\ \mathbf{V}^l(t), & \mathbf{s}^l(t) = 0. \end{cases} \quad (6)$$

Here, $\lambda \in (0, 1)$ is the membrane potential decay coefficient. The reset mechanism adopts a hard reset.

To evaluate the generality of the proposed attack, we employ several neuron models in addition to the standard LIF neuron, including its variant LIF-2, the Integrate-and-Fire

(IF) neuron, and the Parallel Spiking Neuron (PSN) [14]. Detailed configurations of these models are provided in the Supplementary Materials.

Regardless of the neuron model, backpropagation in SNNs requires approximating $\frac{dH}{dx}$ through surrogate gradients. For example, the arctangent (Atan) surrogate gradient function is defined as:

$$\frac{dH}{dx} \approx g(x) = \frac{\alpha}{2 \left[1 + \left(\frac{\pi}{2} \alpha x \right)^2 \right]}, \quad (7)$$

where α controls the sharpness of the surrogate gradient.

4. Methods

4.1. Theoretical Analysis on Gradient Vanishing

$H(x)$ is discontinuous and has zero derivatives everywhere in its continuous domain. Therefore, surrogate gradient is employed to approximate a non-zero and smooth derivative for training or adversarial attack. We define the surrogate gradient as the following general class of functions:

Definition 1. A function $g : \mathbb{R} \rightarrow \mathbb{R}_{\geq 0}$ is a surrogate function if it is even, non-decreasing on the interval $(-\infty, 0)$ and $\int_{-\infty}^{\infty} g(x) dx = 1$

Unlike the definition given by Mukhoty et al. [26], we impose the normalization constraint $\int_{-\infty}^{\infty} g(x) dx = 1$. This property guarantees that the integral of $g(x)$ behaves as an approximation to $H(x)$. As shown in Fig. 1(a), $g(x)$ can take either a narrow and sharp or wide and flat shape; a sharper function makes its integral closer to $H(x)$, implying a more accurate gradient approximation.

However, a sharper $g(x)$ tends to approach 0 more rapidly as $|x|$ increases, which can lead to gradient vanishing. Our motivation is to assign $g(x)$ an appropriate sharpness that closely approximates $H(x)$ while preventing excessive gradient vanishing. To this end, we quantitatively measure the gradient vanishing of $g(x)$ as follows:

$$G(x) = \int_{-|x|}^{|x|} g(t) dt, \quad (8)$$

where $G(x)$ denotes the gradient-vanishing degree of $g(x)$ at position x . Without loss of generality, we define the domain of $G(x)$ as $[0, +\infty)$. It can be observed that $G(x)$ is a monotonically non-decreasing function whose range lies within $[0, 1]$. A larger value of $G(x)$ indicates a higher degree of gradient vanishing.

$G(x)$ serves as a suitable quantitative indicator for measuring the gradient vanishing in surrogate functions. As the surrogate function $g(x)$ becomes sharper, $G(x)$ rises toward 1 more rapidly. For the exact derivative of the Heaviside function $H(x)$, we have $G(x) = 1$ on $\forall x > 0$, which implies that the gradient vanishes everywhere.

We can derive the following theorem about $G(x)$:

Theorem 1. *For any surrogate function $g(x)$, the gradient-vanishing degree function $G(x) = \int_{-x}^x g(t) dt, x \geq 0$ is a concave function on $[0, +\infty)$*

We aim to control the gradient-vanishing degree by adjusting the sharpness of the surrogate function for a given surrogate form. We adopt the Atan surrogate gradient (see Eq. (7)) because it is smooth and has a long tail, which is favorable for stabilizing backpropagation in SNNs. From Theorem 1, we can select an appropriate sharpness parameter α such that the expected gradient-vanishing degree is upper-bounded by a prescribed constant:

Corollary 1. *Let $g(x) = \frac{\alpha}{2[1+(\frac{\pi}{2}\alpha x)^2]}$ and the corresponding gradient-vanishing degree function $G(x) = \int_{-x}^x g(t) dt, x \geq 0$. Assume that x follows a probability distribution $p(x)$ with finite expectation $\mathbb{E}[x] < +\infty$. Then, for any constant $A \in [0, 1]$, the expected gradient-vanishing degree satisfies*

$$\mathbb{E}_{x \sim p(x)}[G(x)] \leq A \text{ if } \alpha \leq \frac{2}{\pi \mathbb{E}[x]} \tan\left(\frac{\pi A}{2}\right) \quad (9)$$

The detailed proof required for this section is provided in the Supplementary Materials.

4.2. Adaptive Sharpness Surrogate Gradient

Based on the theoretical analysis above, ASSG adaptively computes the sharpness parameter across spatial-temporal dimension of every input during adversarial attacks.

For a given input sample \mathbf{x} , an adversarial attack iteratively searches for adversarial examples, forming an optimization trajectory $\{\mathbf{x}_1, \mathbf{x}_2, \dots, \mathbf{x}_k, \dots\}$. \mathbf{x}_k is transformed into the input to H at a specific spatial-temporal dimension: $u_{i,t}^l(\mathbf{x}_k) = V_i^l(t+1) - V_{\text{th}}$ (i denotes the neuron index). Let $p(|u_{i,t}^l|)$ denote the probability distribution of $|u_{i,t}^l|$ during the optimization process. According to Corollary 1, we can compute $\alpha_{i,t}^l$ to constrain the expected upper bound of gradient vanishing throughout optimization trajectory:

$$\alpha_{i,t}^l = \frac{2}{\pi \mathbb{E}[|u_{i,t}^l|]} \tan\left(\frac{\pi}{2} A\right). \quad (10)$$

where $A \in [0, 1]$ is a tunable constant. We replace the inequality in Eq. (9) with an equality, as we prefer $\alpha_{i,t}^l$ to take the maximum admissible value under the constraint $\mathbb{E}_{|u_{i,t}^l| \sim p(|u_{i,t}^l|)}[G(|u_{i,t}^l|)] \leq A$, ensuring that the surrogate gradient approximates $\frac{dH}{dx}$ as closely as possible.

Next, we estimate $\mathbb{E}[|u_{i,t}^l|]$ during adversarial optimization process. ASSG adaptively estimates $\mathbb{E}[|u_{i,t}^l|]$ by maintaining an exponential moving average (EMA) of $|u_{i,t}^l|$, which is then used to dynamically update the sharpness parameter $\alpha_{i,t}^l$ throughout the attack iterations:

$$M_{i,t}^l(\mathbf{x}_{1:k}) = \beta M_{i,t}^l(\mathbf{x}_{1:k-1}) + (1 - \beta) |u_{i,t}^l(\mathbf{x}_k)| \quad (11)$$

$$\alpha_{i,t}^l(\mathbf{x}_{1:k}) = \frac{2}{\pi M_{i,t}^l(\mathbf{x}_{1:k})} \tan\left(\frac{\pi}{2} A\right). \quad (12)$$

where $\beta \in (0, 1)$ is the momentum coefficient, $\mathbf{x}_{1:k}$ denotes the set of points up to the k -th iteration.

ASSG further incorporates an exponential moving average of the absolute deviation of $|u_{i,t}^l|$ as a relaxation term on top of the EMA estimate:

$$M_{i,t}^l(\mathbf{x}_{1:k}) = \beta_1 M_{i,t}^l(\mathbf{x}_{1:k-1}) + (1 - \beta_1) |u_{i,t}^l(\mathbf{x}_k)| \quad (13)$$

$$D_{i,t}^l(\mathbf{x}_{1:k}) = \beta_2 D_{i,t}^l(\mathbf{x}_{1:k-1}) + (1 - \beta_2) |u_{i,t}^l(\mathbf{x}_k) - M_{i,t}^l(\mathbf{x}_{1:k})| \quad (14)$$

$$\alpha_{i,t}^l(\mathbf{x}_{1:k}) = \frac{2}{\pi [M_{i,t}^l(\mathbf{x}_{1:k}) + \gamma D_{i,t}^l(\mathbf{x}_{1:k})]} \tan\left(\frac{\pi}{2} A\right). \quad (15)$$

where $\beta_1, \beta_2 \in (0, 1)$ are the momentum coefficients, γ is the relaxation coefficient. The relaxation term is introduced to slightly reduce $\alpha_{i,t}^l$ by incorporating the second-order moment information of the $|u_{i,t}^l|$ distribution, thereby ensuring that the degree of gradient vanishing remains within the theoretical upper bound.

As shown in Fig. 1(b), $M_{i,t}^l$ and $D_{i,t}^l$ are initialized to M_0 and D_0 . Eq. (13)-Eq. (15) together constitute the adaptive update rule of ASSG, which allows each neuron to self-adjust its surrogate sharpness.

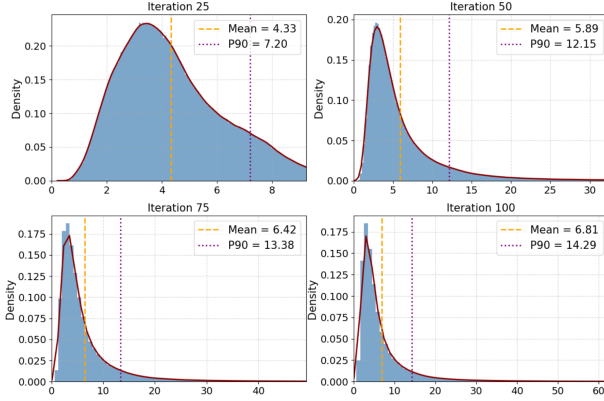


Figure 2. The distribution of the sharpness parameter $\alpha_{i,t}^l$. The vertical lines denote the mean and the 90th percentile (P90), respectively.

In Fig. 2, we visualize the distribution of the sharpness parameter $\alpha_{i,t}^l$ across different spatial-temporal dimensions in ASSG and its evolution along the optimization trajectory. The figure also marks the mean and the 90th percentile (P90) lines. As shown, $\alpha_{i,t}^l$ gradually develops into a unimodal, long-tailed distribution as the iterations proceed, indicating that both sharp and smooth surrogate gradient shapes coexist within the SNN. This highly spatial-temporally heterogeneous and adaptively adjusted backpropagation mechanism ensures stable gradient flow throughout the adversarial optimization trajectory.

4.3. Stable Adaptive Projected Gradient Descent

We find that traditional optimization algorithms, such as PGD and APGD, fail to fully converge even when combined with ASSG for attacking robust SNNs—even after hundreds of iterations, as shown in Fig. 5. This suggests that the input space of SNNs is highly non-smooth and that the gradients remain inaccurate. These observations underscore the need for a more effective adversarial attack optimization algorithm specifically tailored to SNNs—an aspect largely overlooked in prior research.

SA-PGD incorporates both adaptive step size and momentum into adversarial attack optimization, while also considering the L_∞ -norm constraint.

At each attack iteration in SA-PGD, we first compute the L_1 -normalized momentum and the degree of gradient oscillation as follows:

$$\mathbf{m}_k = \beta_m \mathbf{m}_{k-1} + \frac{\nabla_{\mathbf{x}} \mathcal{L}(\mathbf{f}_\theta(\mathbf{x}_k), y)}{\|\nabla_{\mathbf{x}} \mathcal{L}(\mathbf{f}_\theta(\mathbf{x}_k), y)\|_1}, \quad (16)$$

$$\mathbf{v}_k = \beta_v \mathbf{v}_{k-1} + \frac{\nabla_{\mathbf{x}} \mathcal{L}(\mathbf{f}_\theta(\mathbf{x}_k), y)^2}{\|\nabla_{\mathbf{x}} \mathcal{L}(\mathbf{f}_\theta(\mathbf{x}_k), y)^2\|_1}, \quad (17)$$

where β_m, β_v are momentum coefficients. Next we compute the adaptive step size for momentum update based on

\mathbf{v}_k , and apply clipping under the L_∞ -norm constraint to suppress excessively large updates:

$$\mathbf{t}_k = \text{clip}\left(\frac{\mathbf{m}_k}{\sqrt{\mathbf{v}_k} + \xi} \cdot \eta_k, -\eta_k, \eta_k\right), \quad (18)$$

$$\mathbf{x}_{k+1} = \Pi_\varepsilon^\infty(\mathbf{x}_k + \mathbf{t}_k) \quad (19)$$

where η_k is the learning rate, and we adopt the same learning rate adjustment strategy as in APGD. ξ is a small constant for numerical stability. The clipping operator in Eq. (18) limits each element of the update within $[-\eta_k, \eta_k]$, which ensures that no single dimension dominates the adversarial update, maintaining stable and bounded optimization under the L_∞ -norm constraint. Π_ε^∞ projects the updated input back into the feasible region defined by the L_∞ -norm constraint with a perturbation radius of ε .

5. Experiments

5.1. Experimental Setup

We conduct experiments on both static datasets (CIFAR-10 and CIFAR-100 [17]) and a dynamic dataset (CIFAR10-DVS [19]). For each dataset, we employ multiple adversarial training methods to obtain robust models and evaluate the attack success rates (ASR) of the proposed approach. Unlike previous studies [3, 15, 22], we do not consider non-robust SNNs, as these models often achieve 100% ASR when using APGD with large iteration steps and basic gradient approximation methods.

We train robust SNN models using AT, RAT, AT combined with SR (AT+SR), and TRADES. For robust training, we generate adversarial samples with PGD using 5 iterations and a perturbation magnitude $\varepsilon = 8/255$, which is a common practice in current SNN research. The default neuron model in our SNN is the LIF neuron, as described in Eq. (5)-Eq. (6), with a time step of 4 for CIFAR-10/100 and 8 for CIFAR10-DVS. For CIFAR-10/100, the network structure is SEWResNet19 [13], while for CIFAR10-DVS, we use VGG9 [12]. The default input encoding is direct encoding. The detailed experimental setup and parameter configuration are provided in the Supplementary Materials.

5.2. Comparison with State-of-the-art Works

For gradient approximation methods, we compare ASSG with basic STBP (which uses surrogate gradients during training for adversarial attacks) [32] and with recent methods BPTR [8], RGA [3], HART [15], and PDSG [22]. Implementations follow the original papers. For attack methods, APGD serves as the main baseline, with a default of 100 attack iterations and perturbation magnitude $\varepsilon = 8/255$.

Table 1 shows the ASR for different combinations of surrogate gradient approximation methods and attack op-

Table 1. Comparison with the state-of-the-art works. The best results are in bold.

Datasets	Methods	Clean	Attack	BPTR [8]	RGA [3]	PDSG [22]	HART [15]	STBP [32]	ASSG
CIFAR-10	AT	78.69	APGD SA-PGD	66.45 66.85	63.94 65.08	69.31 68.76	77.22 79.49	75.38 75.11	84.06 88.44
	RAT	80.03	APGD SA-PGD	61.81 62.67	61.05 62.45	67.38 66.72	73.15 75.66	70.81 70.99	81.49 86.44
	AT+SR	77.93	APGD SA-PGD	54.51 54.63	52.62 52.65	56.20 55.43	65.77 67.71	60.82 60.37	73.76 77.00
	TRADES	81.06	APGD SA-PGD	59.75 60.00	56.97 57.64	59.15 58.33	70.63 72.47	66.27 66.24	75.91 79.56
CIFAR-100	AT	51.90	APGD SA-PGD	82.83 82.99	82.50 83.07	84.21 84.00	89.88 90.80	88.22 88.26	91.60 93.19
	RAT	55.38	APGD SA-PGD	76.74 76.94	77.28 78.35	79.68 79.43	84.77 86.21	83.33 83.26	87.73 89.64
	AT+SR	52.11	APGD SA-PGD	76.86 76.90	77.80 78.19	78.88 78.37	85.09 85.76	82.84 82.73	86.18 87.68
	TRADES	57.08	APGD SA-PGD	78.89 79.06	78.99 79.39	79.17 78.88	86.07 87.00	84.27 84.15	87.57 89.22
CIFAR10-DVS	AT	79.70	APGD SA-PGD	33.00 32.00	32.10 31.90	33.40 33.10	35.40 34.80	36.10 35.40	47.00 49.10
	RAT	82.50	APGD SA-PGD	31.30 30.60	30.20 29.20	33.20 31.80	34.00 33.20	35.20 34.30	42.50 44.60
	AT+SR	79.40	APGD SA-PGD	31.90 31.20	31.40 31.00	32.50 31.90	34.50 34.60	36.30 35.60	42.50 43.60
	TRADES	76.60	APGD SA-PGD	32.20 31.30	30.70 28.80	32.70 32.00	34.00 33.60	34.20 33.90	36.20 36.80

Table 2. ASR on different network architectures and depths.

Datasets	Architectures	Clean	Attack	BPTR	RGA	PDSG	HART	STBP	ASSG
CIFAR-10	VGG9	82.09	APGD SA-PGD	62.86 62.86	67.15 67.59	67.60 67.04	77.39 79.86	72.37 72.21	83.97 88.16
	SEWResNet19	78.69	APGD SA-PGD	66.45 66.85	63.94 65.08	69.31 68.76	77.22 79.49	75.38 75.11	84.06 88.44
	SEWResNet31	77.50	APGD SA-PGD	65.72 65.72	60.82 61.63	68.38 67.27	75.73 77.90	74.49 74.31	83.18 87.38
	SEWResNet43	74.80	APGD SA-PGD	57.86 56.87	59.25 59.08	66.15 64.73	75.61 77.41	72.79 71.76	88.05 91.43
CIFAR-100	VGG9	54.74	APGD SA-PGD	77.28 77.33	82.16 82.16	81.10 80.63	88.06 88.94	84.26 84.28	89.94 91.77
	SEWResNet19	51.90	APGD SA-PGD	82.83 82.99	82.50 83.07	84.21 84.00	89.88 90.80	88.22 88.26	91.60 93.19
	SEWResNet31	51.02	APGD SA-PGD	82.38 82.68	80.49 81.08	83.86 83.59	88.78 89.59	87.60 87.66	89.74 91.44
	SEWResNet43	49.27	APGD SA-PGD	83.24 83.29	79.37 80.22	84.72 84.46	88.00 88.69	87.66 87.82	89.00 90.60

timization algorithms. A higher ASR indicates a more accurate evaluation of adversarial robustness. ASSG consistently achieves the highest ASR across various datasets and training methods, particularly on CIFAR-10 and CIFAR10-DVS, where ASSG outperforms other gradient approxima-

tion methods by a significant margin (near 10% in 7 cases). When combined with SA-PGD, ASSG further improves ASR over APGD in every experiment. However, SA-PGD shows little benefit when paired with low-quality gradient approximations (BPTR, RGA, PDSG, STBP), indicating

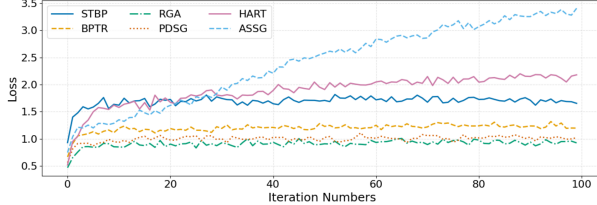


Figure 3. The loss curves of SA-PGD for different gradient approximation methods.

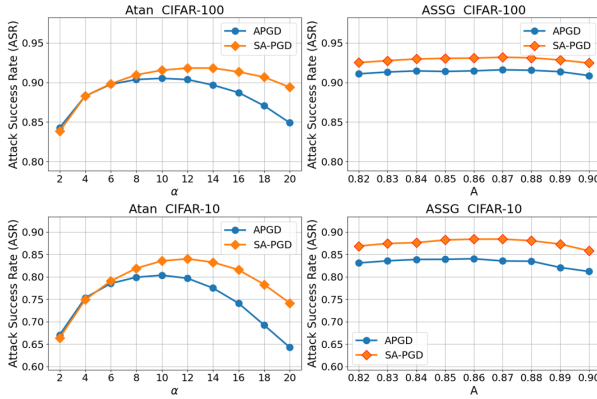


Figure 4. ASR for attacks using Atan surrogate gradients with different values of α and ASSG with different values of A .

that the optimization algorithm and the gradient approximation method mutually influence the effectiveness of adversarial attacks.

Furthermore, we plot the loss curves of SA-PGD on CIFAR-10 for different gradient approximation methods in Fig. 3. As the number of iterations increases, the loss curves of all gradient approximation methods except ASSG tend to converge, while ASSG continues to exhibit an upward trend, further demonstrating its superiority. The loss curves of STBP and HART are higher than that of ASSG in the early stages but are later surpassed by ASSG as the iterations proceed, demonstrating that ASSG dynamically adjusts the spatial-temporal distribution of sharpness parameters. In our configuration, the ASR of RGA and PDSG methods are even lower than that of basic STBP, which contradicts the conclusions of their original papers [3, 22]. However, our results are more reliable, as previous works [3, 15, 22] only compared ASR using PGD with 10 iterations. The higher ASR reported in those studies may simply reflect a faster loss increase during the early attack iterations.

5.3. Ablation Study

Ablation Study on Gradient Approximation. The surrogate gradient function in ASSG is structurally similar to that of Atan, with the key difference being that ASSG uses

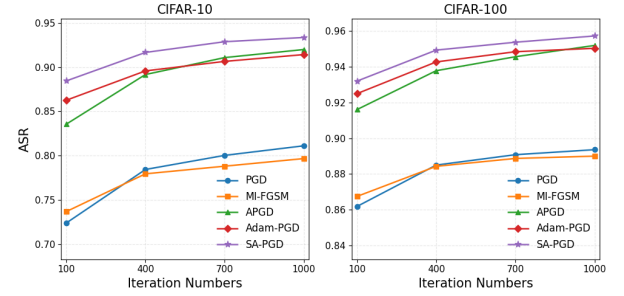


Figure 5. ASR of different attack methods at varying iteration numbers when using ASSG as the surrogate gradient.

the upper bound of gradient vanishing degree, A , as a parameter. ASSG allows SNNs to adaptively adjust the surrogate gradient sharpness parameter $\alpha_{i,t}^l$ in adversarial attacks, whereas Atan uses a fixed sharpness parameter α .

Figure 4 shows the ASR for attacks using Atan surrogate gradients with different values of α and ASSG with different A , with the target model trained using AT. When α is set as a fixed hyperparameter, a small α leads to inaccurate gradients, whereas an excessively large α causes gradient vanishing, resulting in a unimodal relationship between ASR and α . In contrast, ASSG adaptively computes a spatial-temporally heterogeneous $\alpha_{i,t}^l$ for each sample, achieving higher ASR than the manually tuned optimal α . This demonstrates that the input-dependent adaptive adjustment of surrogate gradient sharpness across spatial-temporal dimensions in ASSG plays a crucial role in accurately estimating input gradients.

Ablation Study on Adversarial Attack. We use ASSG with $A = 0.87$ as the surrogate gradient and compare the ASR of multiple attack methods across different numbers of iterations. The update rule in SA-PGD is similar to Adam [16]—incorporating adaptive step sizes and momentum—but it additionally applies per-step L_∞ -norm clipping to the update (see Eq. (18)). To isolate the effect of this clipping, we construct a baseline attack that uses Adam-style optimization for perturbation updates (see Supplementary Materials for details); we denote this variant Adam-PGD. In addition to Adam-PGD, we include the commonly used attacks MI-FGSM [11], PGD, and APGD as baselines. Each attack is evaluated with multiple iteration numbers to ensure a rigorous comparison of convergence behavior and final ASR.

As shown in Fig. 5, the ASR continues to increase slightly for all attack methods even after 1000 iterations. This observation demonstrates the stability of the update dynamics described in Eq. (13)–Eq. (15). Regardless of the optimization algorithm used, ASSG remains stable throughout the iterations and does not collapse into degraded gradient estimates as the attack iterations increase. PGD and

Table 3. ASR on different neuron models, time steps T and encoder.

Datasets	Neuron	T	Encoder	Clean	Attack	BPTR	RGA	PDSG	HART	STBP	ASSG
CIFAR-10	LIF-2	4	Direct	79.68	APGD SA-PGD	63.01 63.36	63.52 63.11	65.82 65.27	71.99 73.50	71.93 73.15	78.30 82.40
	IF	4	Direct	77.21	APGD SA-PGD	67.16 66.83	67.25 67.04	68.92 68.13	64.14 65.22	75.38 76.54	86.51 90.47
	PSN	4	Direct	77.37	APGD SA-PGD	- -	- -	69.51 69.27	44.71 43.43	78.49 78.62	97.25 98.56
	LIF	8	Direct	78.98	APGD SA-PGD	60.69 61.27	59.30 60.37	64.79 64.46	71.92 73.28	70.06 70.20	76.61 79.74
	LIF	4	Poisson	71.81	APGD SA-PGD	55.61 58.59	55.17 59.37	56.34 57.14	61.88 63.60	59.55 60.64	60.70 62.84
CIFAR-100	LIF-2	4	Direct	50.95	APGD SA-PGD	81.88 81.99	84.37 84.00	83.15 83.02	87.02 87.50	86.83 87.38	88.28 89.60
	IF	4	Direct	48.27	APGD SA-PGD	83.82 83.79	86.43 86.25	84.70 84.19	77.22 79.49	87.95 88.75	89.87 91.16
	PSN	4	Direct	48.53	APGD SA-PGD	- -	- -	84.91 84.76	78.61 78.95	90.36 90.61	97.90 98.82
	LIF	8	Direct	51.87	APGD SA-PGD	79.21 79.54	79.76 80.09	81.43 80.97	86.46 87.00	85.07 85.19	87.76 89.14
	LIF	4	Poisson	44.97	APGD SA-PGD	75.45 76.58	75.72 77.48	77.09 77.34	80.64 81.15	80.20 80.73	80.50 81.01

MI-FGSM show notably weaker performance. Adam-PGD, benefiting from its adaptive step-size mechanism, converges faster and achieves higher ASR than APGD at low iteration counts; however, as iterations increase, its ASR drops below APGD. This is because Adam-PGD, lacking per-step L_∞ -norm clipping, may produce updates that deviate excessively from the constrained region, causing instability in later stages. In contrast, SA-PGD, which explicitly incorporates the L_∞ -norm constraint in Eq. (18), achieves the highest ASR across all iteration numbers, clearly demonstrating its superiority.

5.4. Generalizability across Configurations

We also evaluate the generalizability of the proposed method across different configurations, including varying neuron models, network architectures, time steps and encoder. All models in this section are trained by AT.

As shown in Tab. 2, across all network architectures and depths, both ASSG and SA-PGD effectively improve the ASR, demonstrating the excellent applicability of our method to different network structures.

Furthermore, for SNNs based on the SEWResNet19 architecture, we comprehensively evaluate the generalizability of our proposed method in Tab. 3. Since Poisson encoder is a stochastic input transformation, we use Expectation over Transformation (EOT) to compute input gradients during the attack [2], with the number of attack iterations set to 50. To reduce the estimation bias in EOT, the update of the surrogate gradient sharpness in ASSG is frozen

within the EOT loop. In addition, the PSN model differs significantly from conventional neuron models—it has no fixed threshold or reset mechanism—making it incompatible with BPTR and RGA methods.

As shown in Tab. 3, our method performs well across all configurations. ASSG achieves superior attack effectiveness on SNNs with various neuron models and time steps, with its ASR only slightly lower than HART under Poisson encoder. Notably, ASSG attains over 98% ASR on the PSN model, substantially outperforming other gradient approximation methods. In contrast, HART shows significantly weaker attack performance on PSN, highlighting the limitations of gradient approximation methods derived from specific neuron dynamics. In comparison, ASSG computes the adaptive surrogate gradient solely based on the input distribution of the function H , independent of neuron dynamics, thereby exhibiting much stronger generalizability.

6. Conclusion

In this work, we theoretically analyze the gradient vanishing behavior of surrogate functions in SNNs and propose ASSG, an effective gradient approximation method for adversarial attack optimization. Together with the optimization algorithm SA-PGD, it forms a more reliable framework for evaluating the adversarial robustness of SNNs. Extensive experiments demonstrate that our approach consistently outperforms prior methods in both performance and generalizability, advancing the understanding and assess-

ment of robust SNNs.

Moreover, our results reveal that existing studies have overestimated the adversarial robustness of SNNs and underestimated the number of attack iterations required for rigorous robustness evaluation. In current SNN adversarial training, the inner maximization in Eq. (2) is typically approximated using 5–10 steps of PGD with the same surrogate gradients used during training (i.e., STBP). Our findings show that this approximation is far from optimal, severely compromising the effectiveness of adversarial training. Hence, there is a pressing need to rethink how to design efficient and reliable methods for solving the inner maximization problem in SNN adversarial training.

References

[1] Anish Athalye, Nicholas Carlini, and David Wagner. Obfuscated gradients give a false sense of security: Circumventing defenses to adversarial examples. In *International conference on machine learning*, pages 274–283. PMLR, 2018. 1

[2] Anish Athalye, Logan Engstrom, Andrew Ilyas, and Kevin Kwok. Synthesizing robust adversarial examples. In *International conference on machine learning*, pages 284–293. PMLR, 2018. 1, 8, 3

[3] Tong Bu, Jianhao Ding, Zecheng Hao, and Zhaofei Yu. Rate gradient approximation attack threats deep spiking neural networks. In *Proceedings of the IEEE/CVF Conference on Computer Vision and Pattern Recognition*, pages 7896–7906, 2023. 1, 2, 5, 6, 7, 3

[4] Wuque Cai, Hongze Sun, Qianqian Liao, Jiayi He, Duo Chen, Dezhong Yao, and Daqing Guo. Robust spatiotemporal prototype learning for spiking neural networks. *IEEE Transactions on Neural Networks and Learning Systems*, 2025. 1

[5] Nicholas Carlini and David Wagner. Towards evaluating the robustness of neural networks. In *2017 ieee symposium on security and privacy (sp)*, pages 39–57. Ieee, 2017. 2

[6] Francesco Croce and Matthias Hein. Reliable evaluation of adversarial robustness with an ensemble of diverse parameter-free attacks. In *International conference on machine learning*, pages 2206–2216. PMLR, 2020. 2

[7] Mike Davies, Narayan Srinivasa, Tsung-Han Lin, Gautham Chinya, Yongqiang Cao, Sri Harsha Choday, Georgios Dimou, Prasad Joshi, Nabil Imam, Shweta Jain, et al. Loihi: A neuromorphic manycore processor with on-chip learning. *Ieee Micro*, 38(1):82–99, 2018. 1

[8] Jianhao Ding, Tong Bu, Zhaofei Yu, Tiejun Huang, and Jian Liu. Snn-rat: Robustness-enhanced spiking neural network through regularized adversarial training. *Advances in Neural Information Processing Systems*, 35:24780–24793, 2022. 2, 5, 6

[9] Jianhao Ding, Zhiyu Pan, Yujia Liu, Zhaofei Yu, and Tiejun Huang. Robust stable spiking neural networks. In *Proceedings of the 41st International Conference on Machine Learning*, pages 11016–11029. PMLR, 2024.

[10] Jianhao Ding, Zhaofei Yu, Tiejun Huang, and Jian K Liu. Enhancing the robustness of spiking neural networks with stochastic gating mechanisms. In *Proceedings of the AAAI Conference on Artificial Intelligence*, pages 492–502, 2024. 2

[11] Yinpeng Dong, Fangzhou Liao, Tianyu Pang, Hang Su, Jun Zhu, Xiaolin Hu, and Jianguo Li. Boosting adversarial attacks with momentum. In *Proceedings of the IEEE conference on computer vision and pattern recognition*, pages 9185–9193, 2018. 2, 7

[12] Chaoteng Duan, Jianhao Ding, Shiyan Chen, Zhaofei Yu, and Tiejun Huang. Temporal effective batch normalization in spiking neural networks. *Advances in Neural Information Processing Systems*, 35:34377–34390, 2022. 5, 2

[13] Wei Fang, Zhaofei Yu, Yanqi Chen, Tiejun Huang, Timothée Masquelier, and Yonghong Tian. Deep residual learning in spiking neural networks. *Advances in Neural Information Processing Systems*, 34:21056–21069, 2021. 5

[14] Wei Fang, Zhaofei Yu, Zhaokun Zhou, Ding Chen, Yanqi Chen, Zhengyu Ma, Timothée Masquelier, and Yonghong Tian. Parallel spiking neurons with high efficiency and ability to learn long-term dependencies. *Advances in Neural Information Processing Systems*, 36:53674–53687, 2023. 1, 3, 2

[15] Zecheng Hao, Tong Bu, Xinyu Shi, Zihan Huang, Zhaofei Yu, and Tiejun Huang. Threaten spiking neural networks through combining rate and temporal information. In *The Twelfth International Conference on Learning Representations*, 2023. 1, 2, 5, 6, 7

[16] Diederik P Kingma. Adam: A method for stochastic optimization. *arXiv preprint arXiv:1412.6980*, 2014. 7

[17] Alex Krizhevsky, Geoffrey Hinton, et al. Learning multiple layers of features from tiny images. *Technical Report*, 2009. 5

[18] Souvik Kundu, Massoud Pedram, and Peter A Beerel. Hires-snn: Harnessing the inherent robustness of energy-efficient deep spiking neural networks by training with crafted input noise. In *Proceedings of the IEEE/CVF International Conference on Computer Vision*, pages 5209–5218, 2021. 2

[19] Hongmin Li, Hanchao Liu, Xiangyang Ji, Guoqi Li, and Luping Shi. Cifar10-dvs: an event-stream dataset for object classification. *Frontiers in neuroscience*, 11:244131, 2017. 5

[20] Ling Liang, Xing Hu, Lei Deng, Yujie Wu, Guoqi Li, Yufei Ding, Peng Li, and Yuan Xie. Exploring adversarial attack in spiking neural networks with spike-compatible gradient. *IEEE transactions on neural networks and learning systems*, 34(5):2569–2583, 2021. 2

[21] Yujia Liu, Tong Bu, Jianhao Ding, Zecheng Hao, Tiejun Huang, and Zhaofei Yu. Enhancing adversarial robustness in SNNs with sparse gradients. In *Proceedings of the 41st International Conference on Machine Learning*, pages 30738–30754. PMLR, 2024. 2

[22] Li Lun, Kunyu Feng, Qinglong Ni, Ling Liang, Yuan Wang, Ying Li, Dunshan Yu, and Xiaoxin Cui. Towards effective and sparse adversarial attack on spiking neural networks via breaking invisible surrogate gradients. In *Proceedings of the Computer Vision and Pattern Recognition Conference*, pages 3540–3551, 2025. 1, 2, 5, 6, 7, 3

[23] De Ma, Xiaofei Jin, Shichun Sun, Yitao Li, Xundong Wu, Youneng Hu, Fangchao Yang, Huajin Tang, Xiaolei Zhu, Peng Lin, et al. Darwin3: a large-scale neuromorphic chip with a novel isa and on-chip learning. *National Science Review*, 11(5):nwae102, 2024. 1

[24] Aleksander Madry, Aleksandar Makelov, Ludwig Schmidt, Dimitris Tsipras, and Adrian Vladu. Towards deep learning models resistant to adversarial attacks. In *International Conference on Learning Representations*, 2018. 2

[25] Seyed-Mohsen Moosavi-Dezfooli, Alhussein Fawzi, and Pascal Frossard. Deepfool: a simple and accurate method to fool deep neural networks. In *Proceedings of the IEEE conference on computer vision and pattern recognition*, pages 2574–2582, 2016. 2

[26] Bhaskar Mukhoty, Velibor Bojkovic, William de Vazelhes, Xiaohan Zhao, Giulia De Masi, Huan Xiong, and Bin Gu. Direct training of snn using local zeroth order method. *Advances in Neural Information Processing Systems*, 36: 18994–19014, 2023. 1, 3

[27] Bhaskar Mukhoty, Hilal AlQuabeh, and Bin Gu. Improving generalization and robustness in snns through signed rate encoding and sparse encoding attacks. In *The Thirteenth International Conference on Learning Representations*, 2025. 2

[28] Garrick Orchard, E Paxon Frady, Daniel Ben Dayan Rubin, Sophia Sanborn, Sumit Bam Shrestha, Friedrich T Sommer, and Mike Davies. Efficient neuromorphic signal processing with loihi 2. In *2021 IEEE Workshop on Signal Processing Systems (SiPS)*, pages 254–259. IEEE, 2021. 1

[29] Tianyu Pang, Min Lin, Xiao Yang, Jun Zhu, and Shuicheng Yan. Robustness and accuracy could be reconcilable by (proper) definition. In *International conference on machine learning*, pages 17258–17277. PMLR, 2022. 3

[30] Jing Pei, Lei Deng, Sen Song, Mingguo Zhao, Youhui Zhang, Shuang Wu, Guanrui Wang, Zhe Zou, Zhenzhi Wu, Wei He, et al. Towards artificial general intelligence with hybrid tianjic chip architecture. *Nature*, 572(7767):106–111, 2019. 1

[31] Kaushik Roy, Akhilesh Jaiswal, and Priyadarshini Panda. Towards spike-based machine intelligence with neuromorphic computing. *Nature*, 575(7784):607–617, 2019. 1

[32] Yujie Wu, Lei Deng, Guoqi Li, Jun Zhu, and Luping Shi. Spatio-temporal backpropagation for training high-performance spiking neural networks. *Frontiers in neuroscience*, 12:331, 2018. 1, 2, 5, 6

[33] Mengting Xu, De Ma, Huajin Tang, Qian Zheng, and Gang Pan. Feel-snn: Robust spiking neural networks with frequency encoding and evolutionary leak factor. *Advances in Neural Information Processing Systems*, 37:91930–91950, 2024. 2

[34] Nuo Xu, Kaleel Mahmood, Haowen Fang, Ethan Rathbun, Caiwen Ding, and Wujie Wen. Attacking the spike: On the security of spiking neural networks to adversarial examples. *Neurocomputing*, page 131506, 2025. 1

[35] Yinsong Yan, Qu Yang, Yujie Wu, Hanwen Liu, Malu Zhang, Haizhou Li, Kay Chen Tan, and Jibin Wu. Efficient and robust temporal processing with neural oscillations modulated spiking neural networks. *Nature communications*, 16(1):8651, 2025. 1

[36] Bojian Yin, Federico Corradi, and Sander M Bohté. Accurate and efficient time-domain classification with adaptive spiking recurrent neural networks. *Nature Machine Intelligence*, 3(10):905–913, 2021. 1

[37] Hongyang Zhang, Yaodong Yu, Jiantao Jiao, Eric Xing, Laurent El Ghaoui, and Michael Jordan. Theoretically principled trade-off between robustness and accuracy. In *International conference on machine learning*, pages 7472–7482. PMLR, 2019. 3

Towards Reliable Evaluation of Adversarial Robustness for Spiking Neural Networks

Supplementary Material

Overview. The structure of this appendix is as follows:

Sec. S1 provides the proofs of the main theoretical results presented in this paper.

Sec. S2 describes the detailed dynamics of the neuron models used in our experiments.

Sec. S3 presents the full parameter settings for adversarial training and adversarial attacks.

Sec. S4 includes additional experimental results, including:

- Extended SA-PGD loss curves with more iterations.
- Further ablation studies on more training methods.
- Computational overhead comparisons for different gradient approximation methods.
- Experiments analyzing the effect of the relaxation term.

S1. Proofs and Derivations

Theorem 1. For any surrogate function $g(x)$, the gradient-vanishing degree function $G(x) = \int_{-x}^x g(t) dt, x \geq 0$ is a concave function on $[0, +\infty)$

Proof. Since g is even, we have $g(-t) = g(t)$ for all $t \in \mathbb{R}$, and hence

$$G(x) = \int_{-x}^x g(t) dt = 2 \int_0^x g(t) dt, \quad x \geq 0. \quad (\text{S1})$$

We first express the slope of the secant line of G over an interval $[x, y]$ with $0 \leq x < y$ in terms of the average of g on $[x, y]$. Using Eq. (S1), we obtain

$$\begin{aligned} \frac{G(y) - G(x)}{y - x} &= \frac{2 \int_0^y g(t) dt - 2 \int_0^x g(t) dt}{y - x} \\ &= \frac{2}{y - x} \int_x^y g(t) dt. \end{aligned}$$

For any $0 \leq x < y$ and any $t \in [x, y]$, as g is non-increasing on $[0, +\infty)$, we have:

$$g(y) \leq g(t) \leq g(x).$$

Integrating this inequality over $t \in [x, y]$ and dividing by $y - x > 0$, we obtain

$$g(y) \leq \frac{1}{y - x} \int_x^y g(t) dt \leq g(x).$$

This yields

$$2g(y) \leq \frac{G(y) - G(x)}{y - x} \leq 2g(x), \quad 0 \leq x < y. \quad (\text{S2})$$

We now compare slopes on adjacent intervals. Let $0 \leq x < y < z$. Applying Eq. (S2) to the pair (x, y) gives

$$\frac{G(y) - G(x)}{y - x} \geq 2g(y),$$

while applying Eq. (S2) to the pair (y, z) gives

$$\frac{G(z) - G(y)}{z - y} \leq 2g(y).$$

Combining these two inequalities, we obtain

$$\frac{G(y) - G(x)}{y - x} \geq \frac{G(z) - G(y)}{z - y}, \quad 0 \leq x < y < z. \quad (\text{S3})$$

The inequality Eq. (S3) states that the secant slopes of G are nonincreasing as the interval moves to the right. This property is equivalent to concavity. For completeness, we sketch the standard argument.

Fix $0 \leq x < z$ and $\lambda \in (0, 1)$, and define

$$y = \lambda z + (1 - \lambda)x,$$

so that $x < y < z$ and

$$y - x = \lambda(z - x), \quad z - y = (1 - \lambda)(z - x).$$

Substituting into Eq. (S3) and using $z - x > 0$ yields

$$\frac{G(y) - G(x)}{\lambda(z - x)} \geq \frac{G(z) - G(y)}{(1 - \lambda)(z - x)}.$$

Multiplying both sides by $\lambda(1 - \lambda)(z - x) > 0$ gives

$$(1 - \lambda)(G(y) - G(x)) \geq \lambda(G(z) - G(y)).$$

Rearranging terms, we obtain

$$(1 - \lambda)G(y) + \lambda G(y) \geq \lambda G(z) + (1 - \lambda)G(x),$$

that is,

$$G(y) \geq \lambda G(z) + (1 - \lambda)G(x) = \lambda G(z) + (1 - \lambda)G(x).$$

Recalling that $y = \lambda z + (1 - \lambda)x$, this is precisely the concavity inequality

$$G(\lambda z + (1 - \lambda)x) \geq \lambda G(z) + (1 - \lambda)G(x)$$

Hence G is concave on $[0, +\infty)$. \square

Corollary 1. Let $g(x) = \frac{\alpha}{2[1+(\frac{\pi}{2}\alpha x)^2]}$ and the corresponding gradient-vanishing degree function $G(x) = \int_{-x}^x g(t) dt, x \geq 0$. Assume that x follows a probability distribution $p(x)$ with finite expectation $\mathbb{E}[x] < +\infty$. Then, for any constant $A \in [0, 1]$, the expected gradient-vanishing degree satisfies

$$\mathbb{E}_{x \sim p(x)}[G(x)] \leq A \text{ if } \alpha \leq \frac{2}{\pi \mathbb{E}[x]} \tan\left(\frac{\pi A}{2}\right) \quad (\text{S4})$$

Proof. Using the evenness of g , we can rewrite G explicitly as

$$\begin{aligned} G(x) &= 2 \int_0^x g(t) dt \\ &= \alpha \int_0^x \frac{1}{1 + (\frac{\pi}{2}\alpha t)^2} dt \\ &= \frac{2}{\pi} \arctan\left(\frac{\pi}{2}\alpha x\right). \end{aligned}$$

Since G is concave on $[0, +\infty)$ by Theorem 1, Jensen's inequality yields

$$\mathbb{E}_{x \sim p(x)}[G(x)] \leq G(\mathbb{E}[x]) = \frac{2}{\pi} \arctan\left(\frac{\pi}{2}\alpha \mathbb{E}[x]\right). \quad (\text{S5})$$

We now enforce $G(\mathbb{E}[x]) \leq A$:

$$\frac{2}{\pi} \arctan\left(\frac{\pi}{2}\alpha \mathbb{E}[x]\right) \leq A.$$

Since $A \in [0, 1]$, we have $\frac{\pi}{2}A \in [0, \frac{\pi}{2}]$, where \tan is strictly increasing and \arctan is its inverse. Thus the above inequality is equivalent to

$$\arctan\left(\frac{\pi}{2}\alpha \mathbb{E}[x]\right) \leq \frac{\pi A}{2} \iff \frac{\pi}{2}\alpha \mathbb{E}[x] \leq \tan\left(\frac{\pi A}{2}\right),$$

that is,

$$\alpha \leq \frac{2}{\pi \mathbb{E}[x]} \tan\left(\frac{\pi A}{2}\right).$$

Under this condition, we have $G(\mathbb{E}[x]) \leq A$, and hence by Eq. (S5),

$$\mathbb{E}_{x \sim p(x)}[G(x)] \leq G(\mathbb{E}[x]) \leq A,$$

which proves Eq. (S4). \square

S2. Spiking Neuron Models

LIF-2. We use LIF-2 to denote a variant of the LIF neuron model, which has been adopted in prior works such as [3, 8, 10, 15, 21, 22]. The dynamics of LIF-2 are given as follows:

$$\mathbf{V}^l(t+1) = \lambda R(\mathbf{V}^l(t), \mathbf{s}^l(t)) + \mathbf{W}^l \mathbf{s}^{l-1}(t+1), \quad (\text{S6})$$

$$R(\mathbf{V}^l(t), \mathbf{s}^l(t)) = \begin{cases} 0, & \mathbf{s}^l(t) = 1, \\ \mathbf{V}^l(t), & \mathbf{s}^l(t) = 0. \end{cases} \quad (\text{S7})$$

The main difference between LIF-2 and the standard LIF neuron is that LIF-2 does not apply the $1 - \lambda$ normalization factor to the input current.

IF. The IF neuron further simplifies this by setting the decay coefficient to 1:

$$\mathbf{V}^l(t+1) = R(\mathbf{V}^l(t), \mathbf{s}^l(t)) + \mathbf{W}^l \mathbf{s}^{l-1}(t+1), \quad (\text{S8})$$

$$R(\mathbf{V}^l(t), \mathbf{s}^l(t)) = \begin{cases} 0, & \mathbf{s}^l(t) = 1, \\ \mathbf{V}^l(t), & \mathbf{s}^l(t) = 0. \end{cases} \quad (\text{S9})$$

PSN. The PSN is a neuron model that enables parallel processing along the temporal dimension, and its dynamics differ fundamentally from those of conventional neurons [14]. PSN removes the reset mechanism and treats the firing threshold at each time step as a learnable parameter:

$$\mathbf{V}^l = \mathbf{W}_T^l \mathbf{X}^l, \mathbf{W}_T^l \in \mathbb{R}^{T \times T}, \mathbf{X}^l \in \mathbb{R}^{T \times N} \quad (\text{S10})$$

$$\mathbf{S}^l = H(\mathbf{V}^l - \mathbf{B}^l), \mathbf{B}^l \in \mathbb{R}^T, \mathbf{S}^l \in \{0, 1\}^{T \times N} \quad (\text{S11})$$

where \mathbf{X}^l , \mathbf{V}^l and \mathbf{S}^l denote the input current, membrane potential, and spike sequence, respectively, and \mathbf{W}_T^l and \mathbf{B}^l represent the learnable temporal weight matrix and threshold parameters. This formulation allows the membrane potential $\mathbf{V}^l(t)$ at each time step to integrate information from all temporal positions, rather than relying solely on the previous step as in conventional neuron models.

S3. Detailed Experimental Settings

S3.1. Adversarial Training Settings

In this work, we train robust SNN models using commonly adopted adversarial training schemes for evaluation. Both standard adversarial training (AT) and TRADES generate adversarial examples using PGD with a perturbation budget of $\varepsilon = 8/255$, a step size of $\eta = 4/255$, and 5 attack iterations. RAT and AT+SR follow the same AT setup but additionally incorporate their respective regularization terms, with the regularization coefficient set to 0.004 for both methods.

We adopt Temporal Efficient Training (TET) [12] as the loss function and optimize the models using SGD with a momentum of 0.9. All models are trained for 100 epochs. For SNNs using neuron models other than PSN, we employ a triangular surrogate gradient during training:

$$\frac{dH}{dx} \approx 2 \cdot \max \{0, 1 - |x|\} \quad (\text{S12})$$

PSN-based SNNs are trained using the Atan surrogate gradient with $\alpha = 4$.

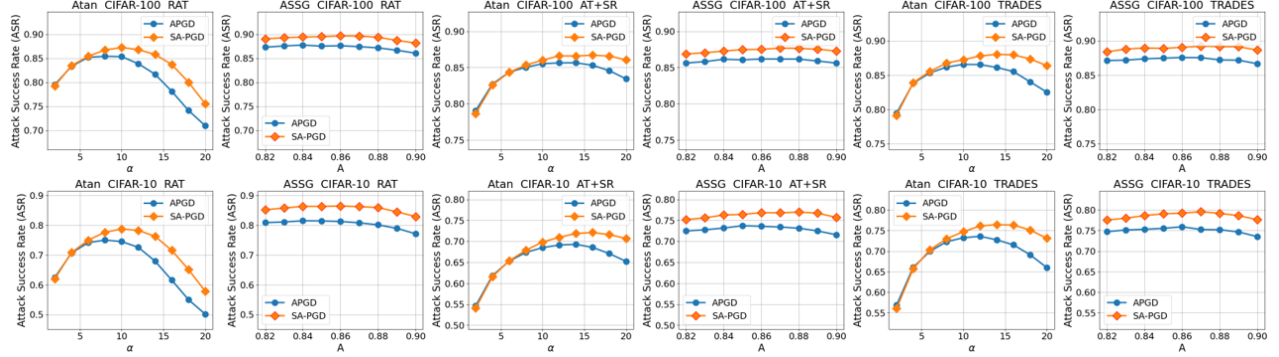


Figure S1. ASR for attacks using Atan surrogate gradients with different values of α and ASSG with different values of A .

Table S1. Computational cost of training one epoch on CIFAR-10

	BPTR	RGA	PDSG	HART	STBP	ASSG
Runtime(s)	7.7	8.0	13.7	11.2	11.3	15.4
Memory Usage(MB)	7161	8171	11265	9473	9473	13577

S3.2. Adversarial Attack Settings

For RGA and PDSG, we follow the parameter settings provided in their original papers [3, 22]. For ASSG, we set $\beta_1 = 0.9$ and $\beta_2 = 0.9$ when Poisson encoding is not used. When Poisson encoding is applied, we instead use $\beta_1 = 0.99$ and $\beta_2 = 0.99$. The initial values of $M_{i,t}^l$ and $D_{i,t}^l$ are set to $M_0 = 1.0$ and $D_0 = 0.0$, respectively, and the relaxation coefficient $\gamma = 1.5$. We search for the optimal value of A within the range $[0.82, 0.9]$ with a step size of 0.01. Although the ASR values of ASSG reported in Tab. 1–Tab. 3 correspond to the best-performing A , Fig. 4 and Fig. S1 demonstrate that the attack performance of ASSG is robust to the choice of A .

For SA-PGD, we set $\beta_m = 0.5$ and $\beta_v = 0.8$. When attacking SNNs with Poisson encoding, we estimate the gradient using the Expectation-over-Transformation (EOT) technique [2], with 10 EOT samples per iteration.

We design Adam-PGD as a baseline for comparison with SA-PGD. The update rule in Adam-PGD follows the Adam optimization mechanism, with an additional projection step to ensure that the updated input remains within the L_∞ constraint:

$$\mathbf{m}_k = \beta_m \mathbf{m}_{k-1} + (1 - \beta_m) \nabla_{\mathbf{x}} \mathcal{L}(\mathbf{f}_\theta(\mathbf{x}_k), y) \quad (\text{S13})$$

$$\mathbf{v}_k = \beta_v \mathbf{v}_{k-1} + (1 - \beta_v) \nabla_{\mathbf{x}} \mathcal{L}(\mathbf{f}_\theta(\mathbf{x}_k), y)^2 \quad (\text{S14})$$

$$\widehat{\mathbf{m}}_k = \frac{\mathbf{m}_k}{1 - \beta_m^k}, \quad \widehat{\mathbf{v}}_k = \frac{\mathbf{v}_k}{1 - \beta_v^k}, \quad (\text{S15})$$

$$\mathbf{x}_{k+1} = \Pi_{\varepsilon}^{\infty} \left(\mathbf{x}_k + \eta_k \frac{\widehat{\mathbf{m}}_k}{\sqrt{\widehat{\mathbf{v}}_k} + \xi} \right) \quad (\text{S16})$$

where η_k adopt the same learning rate adjustment strategy as in APGD and SA-PGD. We set $\beta_m = 0.8$ and $\beta_v = 0.9$ in Adam-PGD.

S4. Additional Results

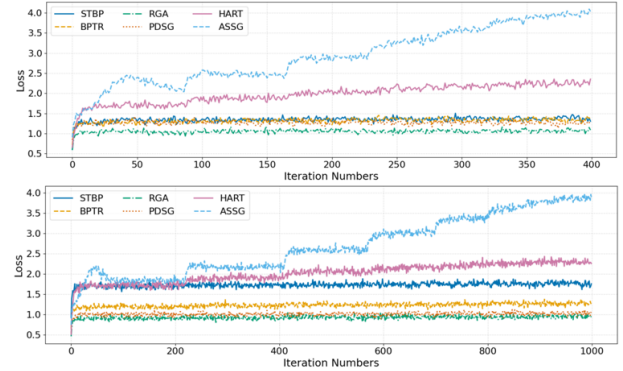


Figure S2. The loss curves of SA-PGD for different gradient approximation methods and iteration numbers.

S4.1. Loss Curves of more Iteration Numbers

We further plot the loss curves of different gradient approximation methods under SA-PGD at 400 and 1000 attack iterations to more comprehensively examine their convergence behavior. As shown in Fig. S2, ASSG only begins to converge when the iteration reaches 1000 steps, demonstrating its ability to continuously and effectively optimize adversarial perturbations. This requirement for extremely large iteration budgets also highlights the inherent difficulty of generating adversarial examples for SNNs.

Table S2. Comparison of ASR between ASSG with and without the relaxation term.

Datasets	Methods	$\gamma = 0$	$\gamma = 0.5$	$\gamma = 1.0$	$\gamma = 1.5$	$\gamma = 2.0$	$\gamma = 2.5$	$\gamma = 3.0$	$\gamma = 3.5$
CIFAR-10	AT	86.33	87.45	87.97	88.44	88.83	88.96	89.16	89.30
	RAT	85.39	85.92	86.32	86.44	86.78	86.95	87.22	87.27
	AT+SR	75.08	76.13	76.87	77.00	77.48	77.68	77.75	77.89
	TRADES	77.00	78.36	78.97	79.59	79.86	80.19	80.49	80.57
CIFAR-100	AT	92.45	92.87	93.14	93.19	93.40	93.58	93.67	93.76
	RAT	89.02	89.44	89.55	89.64	89.75	89.80	89.93	89.89
	AT+SR	86.72	87.22	87.53	87.68	87.87	87.92	87.98	88.11
	TRADES	88.43	88.91	89.05	89.22	89.35	89.40	89.46	89.43

S4.2. Additional Comparative Experiments between Atan and ASSG

In this section, we present additional results on models trained with various adversarial training methods, reporting the ASR for attacks using Atan surrogate gradients with different values of α and ASSG with different values of A . As shown in the Fig. S1, the results across more models further demonstrate that ASSG’s input-dependent, spatio-temporal adaptive adjustment of the sharpness parameter $\alpha_{i,t}^l$ is superior to directly searching for a globally optimal fixed sharpness parameter α .

S4.3. Computational Cost Comparison

All adversarial attacks are implemented and evaluated in PyTorch on a single NVIDIA A100-PCIE-40GB GPU. We compare the memory usage and runtime of different surrogate gradient methods under the same settings. Specifically, we report the GPU memory consumption and time required to execute 100 steps of SA-PGD on a single CIFAR-10 batch (batch size = 256). As shown in the Tab. S1, although ASSG incurs additional memory and runtime due to its spatio-temporally heterogeneous sharpness parameters $\alpha_{i,t}^l$, this overhead remains acceptable given the substantial improvements in attack effectiveness.

S4.4. Effectiveness of the Relaxation Term

ASSG incorporates a relaxation term that leverages second-order moment information to prevent underestimation of $\mathbb{E}[|u_{i,t}^l|]$. Without this term, the computed sharpness parameter $\alpha_{i,t}^l$ may become excessively large, causing the gradient-vanishing degree to exceed the theoretical upper bound. Table S2 presents a comparison of ASR between ASSG with different relaxation coefficients. As the appropriate range for tuning the parameter A depends on factors such as the relaxation coefficient, the dataset, and the neuron model, we use a ternary search over the interval $[0.6, 0.95]$ to identify the optimal A under each configuration.

As shown in Tab. S2, introducing the relaxation term effectively improves the ASR of ASSG. Although the

ASR is relatively robust to the choice of the relaxation coefficient, larger relaxation coefficients generally yield higher ASR. We leave a deeper investigation of this phenomenon—particularly the role of second-order moment information in improving gradient estimation—to future work.